Open Geosciences

Quantifying the scales of spatial variation in gravel beds using terrestrial and airborne laser scanning data

--Manuscript Draft--

Manuscript Number:	OPENGEO-D-18-00122R2
Full Title:	Quantifying the scales of spatial variation in gravel beds using terrestrial and airborne laser scanning data
Article Type:	Research Article
Keywords:	laser scanning; variogram; upscaling; factorial kriging; geomorphology
Corresponding Author:	Guo-Hao Huang, Ph.D. Feng Chia University Taichung, TAIWAN
Corresponding Author Secondary Information:	
Corresponding Author's Institution:	Feng Chia University
Corresponding Author's Secondary Institution:	
First Author:	Guo-Hao Huang, Ph.D.
First Author Secondary Information:	
Order of Authors:	Guo-Hao Huang, Ph.D.
	Peter M. Atkinson, Ph.D.
	Chi-Kuei Wang, Ph.D.
Order of Authors Secondary Information:	
Abstract:	Previous studies measured gravel bed surfaces by terrestrial laser scanning (TLS) and close-range photogrammetry suggested the presence of at least two different scales of spatial variation in gravel bed surfaces. This study investigated the spatial variation of airborne laser scanning (ALS) point clouds acquired in gravel bed. Due to the large footprint of ALS systems, a smoother surface is expected, but there exists some uncertainty over the precise scale of ALS measurement (hereafter referred to as the spatial support). As a result, we applied the regularization method, which is a variogram upscaling approach, to investigate the true support of ALS data. The regularization results suggested that the gravel bed surface described by the ALS is much smoother than expected in terms of the ALS reported measurement scale. Moreover, we applied the factorial kriging (FK) method, which allows mapping of different scales of variation present in the data separately (different from ordinary kriging which produces a single map), to obtain the river bed topography at each scale of spatial variation. We found that the short-range and long-range FK maps of the TLS-derived DSMs were able to highlight the edges of gravels and clusters of gravels, respectively. The long-range FK maps of the ALS data shows a pattern of gravel-bed clusters and aggregations of gravels. However, the short-range FK maps of the ALS data produced noisy maps, due to the smoothing effect. This analysis, thus, shows clearly that ALS data may be insufficient for geomorphological and hydraulic engineering applications that require the resolution of individual gravels.

Dear Dr. Piotr Jankowski,

We are pleased to submit the attached manuscript entitled ‘Quantifying the scales of spatial variation in gravel beds using terrestrial and airborne laser scanning data’, for consideration for publication as a research article to Open Geosciences. We are thankful to the referee's comments. The manuscript has been revised according to the comments.

Thank you very much for your considering our manuscript for potential publication. We look forward to hearing from you.

Correspondence and phone calls about the paper should be directed to Dr. Guo-Hao Huang at the following address, and e-mail address:

Geographic Information System Research Center, Feng Chia University, Taichung 407, Taiwan.
E-mail: stephen@gis.tw

Sincerely,

Guo-Hao Huang, Peter M. Atkinson and Chi-Kuei Wang

Replies to comments for *Quantifying the scales of spatial variation in gravel beds using terrestrial and airborne laser scanning data* submitted to *Open Geosciences Journal*

Reviewer: 1

1. Very interesting work on the application of statistical tools in the assessment of spatial data ALS and TLS. The paper represents scientific level and can be published in Open Geosciences.

Reply: We appreciate the positive feedback from the reviewer. Thank you for your kindly review.

Replies to comments for *Quantifying the scales of spatial variation in gravel beds using terrestrial and airborne laser scanning data* submitted to *Open Geosciences Journal*

Reviewer: 2

1. The manuscript entitled "Quantifying the scales of spatial variation in gravel beds using terrestrial and airborne laser scanning data", by G.H. Huang, P.M. Atkinson and C.K. Wang, presents an interesting work. In general, the manuscript should be acceptable for publication but some problems must be repaired prior to publication. Some suggestions are as follows:

Reply: Thank you for your kindly review. We have revised the manuscript accordingly.

2. Please use different terms in the "Title" and the "Keywords".

Reply: As suggested by the reviewer, we have modified the term of "Keywords" as " laser scanning; variogram; upscaling; factorial kriging; geomorphology".

3. Please rewrite the abstract without technical details.

Reply: As suggested by the reviewer, we have modified "Abstract" section.

3. Please justify convincingly why this manuscript (method, thematology etc) connected with OPENGEO's content and scope. Perhaps the using of proper literature would be helpful. Eg: - Migiros G, Bathrellos GD, Skilodimou HD, Karamousalis T (2011) Pinios (Peneus) River (Central Greece): Hydrological - Geomorphological elements and changes during the quaternary. Open Geosciences, 3 (2): 215-228, doi: 10.2478/s13533-011-0019-1. - Bathrellos GD, Vasilatos C, Skilodimou HD, Stamatakis MG (2009): On the occurrence of a pumice-rich layer in Holocene deposits of western Peloponnesus, Ionian Sea, Greece. A geomorphological and geochemical approach. Open Geosciences, 1 (1): 19-32, doi: 10.2478/v10085-009-0006-7 -etc, etc !!!

Reply: As suggested by the reviewer, we have added the reference of ``Bathrellos GD, Vasilatos C, Skilodimou HD, Stamatakis MG (2009): On the occurrence of a pumice-rich layer in Holocene deposits of western Peloponnesus, Ionian Sea, Greece. A geomorphological and geochemical approach. Open Geosciences, 1 (1): 19-32, doi: 10.2478/v10085-009-0006-7.''

We have added the statements for this reference (Page 13, line 347-349): 'In addition, The FK results demonstrates the possibility of riverbed sediment classification [22, 34] because the FK method could obtain the river bed topography at each scale of spatial variation.'.

4. I propose to the authors to be more specific, explanatory and simplified in order to be easily understandable from the readers, especially in the "results" and "discussion" chapters.

Reply: We appreciate your suggestion and we have made little modification. However, we have attempted to highlight the importance of the true ALS support for describing the gravel bed surface and obtaining the river bed topography at a specific scale by applying the FK method in the previous manuscript. Consequently, the FK method shows the potential of classifying riverbed sediment.

5. It would be useful to be described the aim of this paper.

Reply: As suggested by the reviewer, we have added the statements for describing aims of this study (Page 4, line 94-95): 'The aims of this study are to investigate the true support of ALS data and obtain the river bed topography at each scale of spatial variation.'.

6. I suggest to insert a map with the study area. In this map you would use the principles of cartography (coordinates etc).

Reply: As suggested by the reviewer, we have added the location map of study area in Figure (d).

7. Please use the journal format in the text and the reference list.

Reply: We appreciate your suggestion and the format of reference list are modified as the journal format.

8. Please be careful with the spaces between the words.

Reply: We appreciate your suggestion. We have deleted the redundant spaces between the words.

Replies to comments for *Quantifying the scales of spatial variation in gravel beds using terrestrial and airborne laser scanning data* submitted to *Open Geosciences Journal*

Reviewer: 3

1. Good and well written paper. My the only problem is that paper is not about the gravel bed but about variogram. I see two different possibilities

Reply: Thank you for your detailed comments on our work. We have replied each of the comments below.

2. Paper actually is methodological in the field of geostatisctis, if so title should be changed and problem re-addresses as a geostiatistical with given gravel bed is just a case study example. This is simpler solution but I do not thing that paper will be then suitable for that journal.

Reply: The aims of this study are to investigate the true support of ALS data and obtain the river bed topography at each scale of spatial variation. In order to achieve this, the geostatistical tools of regularization and factorial kriging were employed. Consequently, this study covers the aspects of geosciences, especially in the geomorphology. We think the article title for this study is suitable for Open Geosciences journal.

3. Paper is about gravel bed and then introduction and conclusion must refer to that topic with reduced geostatistics as a part of methodology. Conclusion then should highlight achievements gained by methodological improvements addressed to the topic. I think that this problem is easy to fix by re-structuring the text and add informations about study area, detail description of the problem from the point of view of gravel bed analysis and showing the gaps which weren't solved without proposed methodology

Reply: As suggested by the reviewer, we have modified the "Conclusion" section and highlighted the achievements that can be performed by the FK method.

Quantifying the scales of spatial variation in gravel beds using terrestrial and airborne laser scanning data

Guo-Hao Huang[1*], Peter M. Atkinson[234] and Chi-Kuei Wang[5]

[1]Geographic Information System Research Center, Feng Chia University, Taichung 407, Taiwan

[2]Faculty of Science and Technology, Lancaster University, Bailrigg, Lancaster LA1 4YR, UK

[3]Geography and Environment, University of Southampton, Southampton SO17 1BJ, UK

[4]School of Natural and Built Environment, Queen's University Belfast, Belfast BT7 1NN, Northern Ireland, UK

[5]Department of Geomatics, National Cheng Kung University, Tainan 701, Taiwan

This manuscript is submitted to "Terrestrial, Atmospheric and Oceanic Sciences"

Running title: Quantifying the scales of spatial variation by TLS and ALS

Three Key Points:

1. The FK maps of TLS-derived DSMs capture the grain and form scale.

2. The long-range FK maps of ALS data show the gross patterns of clusters.

3. The short-range FK maps of TLS-derived DSMs can be used in hydrodynamic modelling

[*]Correspondence to Dr. Guo-Hao Huang,
Geographic Information System Research Center, Feng Chia University, Taichung 407, Taiwan.
E-mail: guohao.huang@gmail.com

Tel: 04-24516669 ext. 570

ABSTRACT

Previous studies measured gravel bed surfaces by terrestrial laser scanning (TLS) and close-range photogrammetry suggested the presence of at least two different scales of spatial variation in gravel bed surfaces. This study investigated the spatial variation of airborne laser scanning (ALS) point clouds acquired in gravel bed. Due to the large footprint of ALS systems, a smoother surface is expected, but there exists some uncertainty over the precise scale of ALS measurement (hereafter referred to as the spatial support). As a result, we applied the regularization method, which is a variogram upscaling approach, to investigate the true support of ALS data. The regularization results suggested that the gravel bed surface described by the ALS is much smoother than expected in terms of the ALS reported measurement scale. Moreover, we applied the factorial kriging (FK) method, which allows mapping of different scales of variation present in the data separately (different from ordinary kriging which produces a single map), to obtain the river bed topography at each scale of spatial variation. We found that the short-range and long-range FK maps of the TLS-derived DSMs were able to highlight the edges of gravels and clusters of gravels, respectively. The long-range FK maps of the ALS data shows a pattern of gravel-bed clusters and aggregations of gravels. However, the short-range FK maps of the ALS data produced noisy maps, due to the smoothing effect. This analysis, thus, shows clearly that ALS data may be insufficient for geomorphological and hydraulic engineering applications that require the resolution of individual gravels.

Key words: laser scanning; variogram; upscaling; factorial kriging; geomorphology

1. INTRODUCTION

Characterizing the spatial variation in the gravel bed surfaces is vital for estimating the gravel bed roughness and understanding sediment transportation processes [1]. Previous studies used functions representing spatial variation, such as the variogram, to investigate the fractal properties of gravel bed surfaces and differentiate multiple scales of gravel bed roughness. Most of these studies found that the variogram of gravel bed surfaces revealed a nested structure that contains short-range and long-range components, indicating the presence of physical processes operating at two scales [1-7].

A detailed description of gravel bed surfaces is essential for generating a stable and well-structured variogram. Substantial studies have applied the terrestrial approach, which includes terrestrial laser scanning (TLS) and close-range photogrammetry, to produce fine spatial resolution digital surface models (DSMs) of gravel beds within small spatial extent [2, 3, 8-11]. However, using the terrestrial approach to measure gravel bed surfaces over large areas is costly and time-consuming [12]. Thus, the terrestrial approach is not suitable for providing a synoptic analysis of gravel bed roughness in a whole river section. In recent years, several studies have used the airborne approach, which includes airborne laser scanning (ALS), aerial photogrammetry and unmanned aerial systems (UAS), to obtain elevation data over long reaches of gravel-bed rivers [5, 13-16]. The terrestrial approach is able to achieve a spatial resolution of millimetres, and the spatial resolution of data acquired by the airborne approach is typically tens of centimetres [12]. As a result, it is expected that gravel bed surfaces described by the airborne approach will be spatially smoother. Before using the airborne approach to estimate the variation in gravel bed surfaces, it is, therefore, crucial to explore the effect of the change of measurement scale on the gravel bed surface data, spatial characterisations and roughness obtained through ALS.

In geostatistics, the support refers to the space on which an observation is defined and the measurements are the integrals of the spatial variation over the support [17]. It is known that the geostatistical method of regularization can be used to explore the change of support, particularly, upscaling [18, 19]. The regularization method is performed by scaling the variogram model derived from the point support, so no actual measurements over the areal support are required. Huang and Wang [5] applied the regularization method to TLS-derived DSMs and investigated the fractal properties of gravel bed surface by comparing the regularized TLS variogram and variograms of the ALS point clouds (areal support). However, the smoothing effect in ALS is not fully addressed in Huang and Wang [5]. In this study, we explore the smoothing effect of ALS by regularizing the TLS variogram over different supports and comparing this to variograms of the ALS point clouds.

Most studies of characterizing the spatial variation in the gravel bed surfaces were conducted over small sampling areas, it was suggested that gravel bed roughness reflects the subgrain scale [2] or grain-form scale [7] by comparing the characteristic grain size (e.g. d_{50} or d_{84}) with the short range parameter of a nested variogram. However, it is known that the characteristic grain size is

readily affected by the extent of sampling area [2]. Consequently, a filtering method that is capable of generating spatially river bed topography at each scale of spatial variation, as captured in a nested variogram of the gravel bed surface, can facilitate the interpretation of gravel bed roughness.

Factorial kriging (FK) is a spatial filtering method in geostatistics that can distinguish multiple scales of spatial variation in a physical process [20-22]. It has been applied in a variety of domains, including image processing [22, 23], water contamination analysis [24], seismic data analysis [25], health risk analysis [26], and the delineation of gravel-bed clusters [22]. Unlike ordinary kriging (OK), which creates a single predicted map whatever the scales of spatial variation in the data, the FK method acts as a multiple-pass filter (i.e. low-pass and high-pass filters) to generate multiple predicted maps according to the corresponding spatial scales (i.e. short-range and long-range components) represented in the nested variogram, and the data. The FK filter coefficients are data-dependent and are determined by the variogram calculated from the spatial data. It is, thus, of interest to observe the FK maps produced by gravel bed surface data from such systems.

To date, few studies have been conducted to discover the features that represent the bed topography at the individual scale of gravel bed roughness and evaluate the effect of the larger support when applying ALS to gravel beds. The aims of this study are to investigate the true support of ALS data and obtain the river bed topography at each scale of spatial variation. The geostatistical method of regularization was employed to convolve the variogram obtained from TLS-derived DSMs data with the measurement process pertinent to the TLS. We then compared the regularized TLS variogram with the observed ALS variogram to obtain a clear understanding of the true support of ALS data. Moreover, we use the FK method to map the multiple scales of spatial variation in the quasi-point support data (i.e. TLS-derived DSMs) and areal support data (i.e. ALS point clouds). The OK method was also applied to the two types of data and the comparison of the FK and OK results were discussed.

2. METHODOLOGY

2.1 Variogram

Geostatistics is based on the theory of Regionalized Variables (ReV) in which spatial data are treated as regionalized variables, that is, realizations of a Random Function (RF). A RF $Z(\mathbf{x})$ is nothing more than the spatial equivalent of a Random Variable (RV) Z in which Z is a function of spatial location $\mathbf{x}$. The expected values of the RF are spatially dependent, which means that near observations are more related than distant observations [20]. The variogram parameterizes the RF, effectively extending the concept of variance (for a RV) to space.

The variogram is a basic tool in geostatistics and has been widely used to quantify the spatial variability of gravel bed surfaces [1-7, 22, 27]. The empirical variogram, which is half the mean

squared difference of paired data points separated by the lag vector $\mathbf{h}$, can be represented as follows:

$$\hat{\gamma}(\mathbf{h}) = \frac{1}{2N(\mathbf{h})} \sum_{i=1}^{N(\mathbf{h})} [z(\mathbf{x}_i) - z(\mathbf{x}_i + \mathbf{h})]^2 , \quad (1)$$

where $\hat{\gamma}(\mathbf{h})$ is the semivariance, the lag vector $\mathbf{h}$ is the separation between two point pairs, $N(\mathbf{h})$ is the number of data points separated by the lag vector $\mathbf{h}$ and $z(\mathbf{x}_i)$ is the bed elevation at the location $\mathbf{x}_i$. Robert [7] suggested using a detrending procedure to remove the spatial bias caused by the slope of gravel beds: all the TLS-derived DSMs and their ALS counterparts were linearly detrended by a planar surface in this study.

The empirical variogram consists of a set of semivariances $\hat{\gamma}(\mathbf{h})$ at discrete lags. To use the variogram information in the geostatistical operations of OK, FK and regularization, a theoretical variogram model must be fitted to the empirical variogram and it is the parameters of this fitted model that are then used in the operations. The fitted model must be so-called "permissible" or conditional negative semidefinite (CNSD) to ensure that negative prediction variances do not occur [19]. The variogram calculations were performed by the gstat package in the R software.

2.2 Regularization

The geostatistical operation of regularization of the variogram model is based on the change of support concept and is equivalent to spatial convolution in image processing [18, 19]. It can be used to estimate the regularized variogram on an areal support when only point support data are available. Journel and Huijbregts [18] showed that the regularized variogram on areal support v can be estimated from the theoretical point support variogram under the assumption of stationarity using the following formula:

$$\gamma_v(\mathbf{h}) = \bar{\gamma}(v, v_{\mathbf{h}}) - \bar{\gamma}(v, v), \quad (2)$$

where $v_{\mathbf{h}}$ denotes the areal support v translated by lag vector $\mathbf{h}$. The block-to-block variogram $\bar{\gamma}(v, v_{\mathbf{h}})$ is the double integral of the point support variogram between areal support v and areal support $v_{\mathbf{h}}$, separated by lag $\mathbf{h}$, which is expressed as $\bar{\gamma}(v, v_{\mathbf{h}}) = \frac{1}{v^2} \int_v \int_v \gamma(\mathbf{x} - \mathbf{x}_{\mathbf{h}}) \mathrm{d}\mathbf{x} \mathrm{d}\mathbf{x}_{\mathbf{h}}$. The within-block variogram $\bar{\gamma}(v, v)$, is the double integral of the variogram within areal support v, and is

140 represented by $\bar{\gamma}(v,v) = \frac{1}{v^2}\int_v\int_v \gamma(\mathbf{x}-\mathbf{x}')\mathrm{d}\mathbf{x}\mathrm{d}\mathbf{x}'$. Both are estimated through numerical approximation

141 (i.e., averaging of semivariances between discrete points sampled across each support).

142 **2.3 Ordinary kriging**

143 Ordinary kriging (OK) has been used widely to interpolate digital elevation data and so it is
144 introduced only briefly here. OK is the best linear unbiased predictor (BLUP) and has been found to
145 be robust to a wide variety of data properties [19]. The ordinary kriging prediction $\hat{Z}(\mathbf{x_0})$ is a
146 linear-weighted moving average of the available N data points, which can be expressed as follows:

147 $$\hat{Z}(\mathbf{x_0}) = \sum_{i=1}^{N} \lambda_i z(\mathbf{x_i}), \tag{3}$$

148 where λ_i represents the weight assigned to the point at the location $\mathbf{x}_i$. To ensure that the kriging
149 prediction is unbiased, the weights in Eq. (3) sum to one: $\sum_{i=1}^{N}\lambda_i = 1$. OK also minimizes the
150 prediction variance, which is represented by the following:

151 $$\begin{aligned} var[\hat{Z}(x_0)] &= E[\{\hat{Z}(\mathbf{x}_0) - Z(\mathbf{x}_0)\}^2] \\ &= 2\sum_{i=1}^{N}\lambda_i\gamma(\mathbf{x}_i,\mathbf{x}_0) - \sum_{i=1}^{N}\sum_{j=1}^{N}\lambda_i\lambda_j\gamma(\mathbf{x}_i,\mathbf{x}_j) \end{aligned} \tag{4}$$

152 Eq. (4) leads to the system of OK equations including $N+1$ equations and $N+1$ unknowns, which
153 is given by

154 $$\begin{aligned} &\sum_{j=1}^{N}\lambda_j\gamma(\mathbf{x}_i,\mathbf{x}_j) + \psi(\mathbf{x}_0) = \gamma(\mathbf{x}_i,\mathbf{x}_0) \quad \text{for i = 1, 2,…, } N \\ &\sum_{i=1}^{N}\lambda_i = 1 \end{aligned} \tag{5}$$

155 where $\psi(\mathbf{x}_0)$ is a Lagrange multiplier and it is introduced to achieve the minimization. The system
156 of OK equations (Eq. (5)) are solved to provide the weights λ_i needed in Eq. (3).

157 **2.4 Factorial kriging**

158 In OK, $Z(\mathbf{x})$ is predicted from the available data and variogram model as a whole. However, in
159 FK the predictions are derived from the spatial components in the nested variogram separately. In

other words, each spatial component $\hat{Z}^k(\mathbf{x}_0)$ can be predicted by a linear-weighted moving average of the available N data points:

$$\hat{Z}^k(\mathbf{x}_0) = \sum_{i=1}^{N} \lambda_i^k z(\mathbf{x}_i) \quad (6)$$

where the λ_i^k are the weights applied to the available data. For the k components, the weights λ_i^k must sum to 0 to ensure unbiased prediction [19]. Moreover, the variogram can be represented as a set of basic variograms for FK. In this study, the nested variogram of $Z(\mathbf{x})$ is expressed by

$$\gamma(h) = b^0 g^0(\mathbf{h}) + b^1 g^1(\mathbf{h}) + b^2 g^2(\mathbf{h}) \quad (7)$$

where $g^0(\mathbf{h})$, $g^1(\mathbf{h})$ and $g^2(\mathbf{h})$ represent the nugget model, the spherical model with a short range, and the spherical model with a long range, respectively. FK also minimizes the prediction variance, which leads to the FK equations for each component k below:

$$\begin{aligned} \sum_{j=1}^{N} \lambda_j^k \gamma(\mathbf{x_i}, \mathbf{x_j}) \; - \; \psi^k(\mathbf{x_0}) &= b^k g^k(\mathbf{x}_i, \mathbf{x_0}) \quad \text{for } i = 1, 2, \ldots, N \\ \sum_{i=1}^{N} \lambda_i^k &= 0 \end{aligned} \quad (8)$$

The system of FK equations is solved to obtain the weights λ_i^k needed in Eq. (6) for k th component.

3. FIELD SITES AND DATA

3.1 The Nanshih Creek test site

The study area is at a 700 m long section of the Nanshih Creek (24°54'10"N and 121°33'24"E), in northern Taiwan (Figure 1 (a). Nanshih Creek is unregulated with a mean discharge of 40 m^3s^{-1} outside the peak flood period. The gravel bed in Figure 1 is occasionally submerged and migrated due to severe flooding caused by typhoons which occur between May and November of each year.

3.2 Terrestrial laser scanning

A TLS survey was conducted on the six field sites, which are denoted as S1 to S6 in Figure 1a, on June 9th, 10th, and 11th 2009. Figure 1(b and c) shows the field photos of S4 and S6, respectively,

which are the two sites with the largest gravels and smallest gravels among S1 to S6. The sampling area for S1 to S6 is 6 m × 6 m.

The six sites were scanned by a FARO Photon 80 laser scanner with a nominal measurement accuracy of 2 mm. Hodge et al. [9] and Wang et al. [11] have suggested that a multiple scanning strategy could reduce the number of data voids caused by obstruction due to large grains. Therefore, we performed four scans on the middle of the edge of the 6 m × 6 m sampling area for each field site. A fine spatial resolution setting, providing a point spacing of 3 mm at 10 m distance from the scanner, was used for each scan. Each individual scan took about half an hour including the setup, and generated more than 10 million points. Because each scan has its own local Cartesian coordinate system, a registration operation was performed with the aid of identifying four spherical targets (shown in Figure 1(c)) in each scan, and the FARO SCENE software was used to merge the four scans for each field site into a single coordinate system. Except for manual removal of a few distant points or spurious data points returned from aerosols, no other filtering was applied to the merged scan data for each field site. Finally, the two-stage mean-based filter developed by Wang et al. [11] was applied to the merged scan data to generate the TLS-derived DSMs with a spatial resolution of 1 cm. The TLS-derived DSMs are shown in Figure 2.

3.3 Airborne laser scanning

The ALS survey was performed on May 7th 2009 along the river channel, using an Optech ALTM 3070 system mounted in a helicopter. The flying speed was 50 knots, the scan angle 17° and the pulse rate 70 kHz. The nominal elevation and horizontal accuracies of the Optech ALTM 3070 are 15 and 32.5 cm, respectively. The footprint of ALS can be derived from the beam divergence of ALS and flying altitude [28]. The beam divergence is 0.7 mrad for the Optech ALTM 3070 and the flying altitude is 650 m, so the nominal footprint size of the ALS is 45 cm in this study. The average point cloud density is 247 pts m^{-2} by the helicopter with repeated passes. Except for manual removal of a few extreme high points from the ALS dataset, no other filtering was applied to the ALS dataset.

In addition, aerial photos were also collected by a medium-format digital camera, integrated with the Optech ALTM 3070, simultaneously with laser scanning in order to generate the georectified orthophotos with a spatial resolution of 5 cm × 5 cm (see Figure 1).

The six field sites are not easily accessible and no flood event occurred after the ALS survey, which suggested that there should be no noticeable disturbance of the gravel-bed surface within one month period between the ALS survey and in situ TLS measurements. The ALS point clouds were extracted based on the extents of the six field sites. The colour maps of the ALS point clouds for S1 to S6 are shown in Figure 2.

4. RESULTS

4.1 Variogram

The empirical variograms of the detrended TLS-derived DSMs and ALS counterparts for S1 to S6 are shown in Figure 3. The lag intervals of the TLS-derived DSMs and ALS counterparts are 1 cm and 10 cm, respectively. Due to the small lag distance, the dots representing the variograms of the TLS-derived DSMs appear as lines in Figure 3(a-f).

The detrended variograms of S1 and S5 (denoted as black dots in Figure 3(a), (e), (g) and (k)) showed a monotonically increasing semivariance in the largest lags. This shows that a planar trend was not sufficient to remove the trend from these the gravel bed surfaces. A stable estimate of fractal dimension can be obtained if the stationarity prerequisite is fulfilled [2]. Our results indicate that sometimes higher degree polynomial trend surfaces (e.g. the quadratic surface) are needed to remove the trend in the gravel bed surface data. As a result, we removed a quadratic trend from the gravel bed surfaces at sites S1 and S5 such that the empirical variogram reached a plateau (denoted as the grey dots in Figure 3(a), (e), (g) and (k)).

The variograms of the TLS-derived DSMs shown in Figure 3(a)-(f) and variograms of the ALS point clouds shown in Figure 3(g)-(i) show two distinct scales, which are consistent with the observations in previous studies [2, 4-7]. However, the variograms of the ALS point clouds shows a single scale in Figure 3(j)-(l). The empirical variograms exhibited with two distinct scales were fitted with a permissible double spherical model, which is represented as grey dashed lines in Figure 3(a)-(i). The variograms of the ALS point clouds in S4, S5 and S6 were fitted well by a single spherical model in Figure 3(j)-(l). Table 1 lists the parameters of the theoretical variogram models. The nugget variances of the variograms fitted to the TLS-derived DSMs are zero. This is expected due to the very high measurement accuracy of TLS data. As observed in Table 1, S4 and S6 have the largest and smallest ranges of the first spherical model fitted to the TLS variograms, respectively. The largest and smallest ranges of the second spherical model were observed for S2 and S4, respectively.

The variograms of the ALS point clouds exhibit a concave upwards form at small lags (Figure 3(g), (h), (i), and (j)), which implies that ALS measurements over-smooth the gravel bed surface. Compared to the variograms of the TLS-derived DSMs, the variograms of ALS counterparts have smaller semivariances. This is expected as a function of the spatial convolution of the gravel bed surface with the larger measurement support (i.e., the large footprint of ALS). Larger semivariances were observed in the variograms (TLS-derived DSM and ALS point clouds) of S4 (Figure 3(d) and (j)). We suggest that the less spatially organized gravels here lead to greater local variance after detrending in S4, which can be seen in Figure 2(d) and (j). The tiny gravels in S6 generate the small range of the long-range variogram component of the TLS-derived DSM observable in Figure 1(c) and Figure 3(f), also repeated in the variogram of ALS counterpart in Figure 3(l).

4.2 Regularization

The variograms of the TLS-derived DSMs were regularized over the circular ALS support of 45 cm. The 1 cm × 1 cm rectangle cell of the TLS-derived DSM is approximated as a (quasi-)point (it is extremely small relative to the ALS support). Figure 4 shows a comparison of the regularized TLS variograms (denoted as grey dashed lines) and the observed variograms of the ALS point clouds (black dots).

To enable a direct comparison, the regularized variograms were shifted upwards by adding the nugget variances in the theoretical variogram of the ALS point clouds in Table 1. We expect a high agreement between the regularized variogram over a support of 45 cm and the observed variogram of the ALS point clouds. However, the fit is clearly poor in Figure 4(a), (b), (c), (e), and (f). Therefore, we altered the support for regularization until a best fit was obtained between the regularized TLS and the observed ALS variograms. The support that provided the best fit was 66 cm, corresponding to a flying height of 950 m. The dark grey dashed lines in Figure 4 show the regularized TLS variograms over support of 66 cm. Better agreement between the regularized variogram over support of 66 cm and variogram of the ALS point clouds are shown in Figure 4(a), (b), (c), (e), and (f). This demonstrates that the ALS is over-smoothing the gravel bed surfaces, even more than the already coarse support of 45 cm. The experiment performed here demonstrates that the actual support of the ALS is actually closer to 66 cm.

The regularized variogram over support of 45 cm in S4 seems to have a better agreement with the overserved ALS variogram in Figure 4(d). According to Jutzia and Stillab [29], we postulate that the ALS is able to discriminate the large gravels and the surrounding ground in S4, which reduces the over-smoothing effect.

As shown in Figure 4(f), the regularized variogram over the supports of 45 cm and 66 cm are both close to the variogram of the ALS point clouds in S6. This implies that the flat gravel bed surface, which can be seen in Figure 1(c), is already very smooth so that the over-smoothing effect caused by the ALS does not alter greatly the variogram of the ALS point clouds in this case.

4.3 Ordinary kriging

Only the ALS point clouds of S1, S2, and S3 required the fitting of a double spherical model, and OK and FK were performed only for these three sites. The OK maps with a spatial support of 1 cm × 1 cm predicted using the detrended TLS-derived DSMs of S1, S2, and S3 are shown in Figure 5(a), 6(a), and 7(a), respectively. The OK maps with support of 10 cm × 10 cm calculated from the detrended ALS point clouds of S1, S2, and S3 are shown in Figure 5(d), 6(d), and 7(d), respectively. The coverage of the TLS-derived DSMs is nearly 100%, and most OK maps of the TLS-derived DSMs have the same values as the detrended TLS-derived DSMs. Furthermore, it is noted that the OK maps of the ALS point clouds show the variation at a large range and the edges of individual gravels disappear. Compared to the colour maps of the ALS point clouds in Figure 2, the

OK maps of the ALS point clouds seems to represent the spatial relationship of clusters of gravels (Figure 5(d), 6(d), and 7(d)).

4.4 Factorial kriging

The maps predicted by FK of the long-range variogram component with a support of 1 cm × 1 cm from the detrended TLS-derived DSMs of S1, S2, and S3 are shown in Figures 5(b), 6(b), and 7(b), respectively. The maps predicted by FK of the long-range variogram component with a support of 10 cm × 10 cm calculated from the detrended ALS point clouds of S1, S2, and S3 are shown in Figures 5(e), 6(e), and 7(e), respectively. The ring clusters can be observed in Figure 6(b) and 7(b), respectively. It can be observed that the long-range structures in the gravel bed surfaces are clear from the pattern of clusters and aggregations of gravels in Figures 5(b), 6(b), and 7(b). It can be seen that the long-range FK maps of the ALS point clouds show smoother long-range structure compared to the long-range FK maps of the TLS-derived DSMs. Moreover, we found that the long-range FK maps of the ALS point clouds shown in Figures 5(e), 6(e), and 7(e) resemble the OK maps in Figures 5(d), 6(d), and 7(d).

The short-range FK maps with a support of 1 cm × 1 cm calculated from the detrended TLS-derived DSMs of S1, S2, and S3 are shown in Figures 5(c), 6(c), and 7(c), respectively. The short-range FK maps with a support of 10 cm × 10 cm calculated from the detrended ALS point clouds of S1, S2, and S3 are shown in Figures 5(f), 6(f), and 7(f), respectively. We found that the edges of gravels were clear in Figures 5(c), 6(c), and 7(c), which implies that local details of the gravel bed surface could be detected by FK. However, the short-range FK maps of the ALS point clouds show a noisy pattern only.

4. DISCUSSION

This research focused on using the variogram to quantify the scales of spatial variation in the gravel bed surfaces acquired by TLS and ALS. Although a large number of studies have suggested applying planar detrending to remove the large scale trend, such as the slope of gravel beds, before variogram calculation [2-7], the variograms shown in Figure 3(a), (e), (g) and (k) indicate that sometimes higher degree polynomial trend surfaces (e.g. the quadratic surface) are needed to remove the trend in the gravel bed surface data. It is necessary to achieve a bounded variogram (i.e., which reaches a plateau) because the monotonically increasing semivariance in the largest lags would lead to underestimation of the gravel bed roughness (i.e. the fractal dimension $D = 3 - b/2$), which is calculated by the slope of the log-log variogram.

Many studies showed the potential of ALS for characterizing the surface roughness across large areas [5, 30-32]. Comparison of the regularized TLS variogram with the observed variograms of the ALS point clouds in Figure 4 shows that the actual support of ALS is closer to 66 cm (i.e. footprint at the flying altitude of 950 m) rather 45 cm, which provides the evidence that the gravel bed surface described by the ALS is much smoother than expected in terms of the ALS reported measurement scale. As a result, it is crucial to evaluate the smoothing effect caused by ALS, for example, if the intention is to use such a gravel bed surface for geomorphological applications or hydrodynamic modelling.

Nested variograms and FK were used to separate the spatial variation in gravel bed surfaces into two components. We found that short-range FK of the TLS-derived DSMs in Figure 5(c), 6(c), and 7(c) highlighted the edges of gravels and long-range FK of the TLS-derived DSMs in Figure 5(b), 6(b), and 7(b) revealed the patterns of individual and clusters of gravels. These results indicate that the short-range and long-range components of FK usefully correspond to the bed topography at grain scale and form scale, respectively. It is an important finding because we can identify the bed topography at each scale of gravel bed roughness without using the characteristic grain size now. Furthermore, the FK method is applicable to gravel bed surface data obtained by other measurement techniques.

Short-range FK of the ALS point clouds had little utility because it appears as noise. Long-range FK of the ALS point clouds appears to be smoother than that of the TLS-derived DSMs. This shows that the very large footprint of the ALS data could only be used to extract the bed topography at form scale. It is also noted that the OK maps of the ALS point clouds resemble the long-range FK of the ALS point clouds, which could be considered as an approximation.

As mentioned in Rameshwaran et al. [33], it is difficult to obtain a bed topography which coincides with a specific roughness scale in hydrodynamic modelling. The FK results presented here are a good candidate for hydrodynamic modelling. The short-range and long-range FK maps of TLS-derived are able to represent the bed topography at grain and form scale, respectively and this

has potential application in hydrodynamic modelling where it is desirable to isolate particular scales of variation. In addition, The FK results demonstrates the possibility of riverbed sediment classification [22, 34] because the FK method could obtain the river bed topography at each scale of spatial variation.

5. CONCLUSION

Within this study, we explored the effect of a change of support on gravel bed surface data acquired from TLS and ALS, using geostatistical regularization. Although a smoother gravel bed surface measured by ALS is expected due to the large footprint, comparison of the highly controlled regularized TLS variogram with the observed variogram of the ALS point clouds demonstrated unambiguously that gravel bed surfaces acquired by the ALS are over-smoothed, which means that the spatial variation of such gravel bed surface is less than would be expected based on the ALS reported measurement scale. This has important implications for those wishing to use ALS data for geomorphological or hydrodynamic modelling applications.

The FK maps of the TLS-derived DSMs and ALS point clouds were demonstrated for mapping the multiple scales of spatial variation evident in the empirical variograms. We found that the edges of gravels and both individual and clusters of gravels were the major features in the short-range and long-range FK of the TLS-derived DSMs, respectively, which indicates that the data capture the grain and form scale. This suggests that the short-range FK of the TLS-derived DSMs has potential application in hydrodynamic modelling where the desire is to isolate the bed topography at specific scales. In addition, the short-range FK of the TLS-derived DSMs implies the possibility of automated riverbed sediment classification.

The long-range FK maps of the ALS point clouds show the gross patterns of clusters and aggregations of gravel. However, the short-range FK maps of the ALS point clouds produced a noisy pattern with little information content due to the smoothing effect. This analysis, thus, shows clearly that ALS data may be insufficient for geomorphological and hydraulic engineering applications that require the resolution of individual gravels in certain gravel bed surfaces. The downscaling technique may be applied on the ALS data for deriving the variograms on the point support in order to obtaining the small scale of spatial variation in the gravel bed. Caution and investigation of the appropriateness of the technique for the application in hand is advised.

Acknowledgements

Acknowledge any contributions not in the nature of authorship or funding sources here.

REFERENCES

[1] Nikora V.I., Goring D.G., Biggs B. J. F., On gravel-bed roughness characterization. Water Resour. Res., 1998, 34, 517–527.

[2] Butler J.B., Lane S.N., Chandler J.H., Characterization of the structure of river-bed gravels using two-dimensional fractal analysis. Math. Geol., 2001, 33, 301–330.

[3] Carbonneau P.E., Lane S.N., Bergeron N.E., Cost-effective non-metric close-range digital photogrammetry and its application to a study of coarse gravel river beds. Int. J. Remote Sens., 2003, 24, 2387–2854.

[4] Hodge R., Brasington J., Richards K., Analysing laser-scanned digital terrain models of gravel bed surfaces: linking morphology to sediment transport processes and hydraulics. Sedimentology, 2009a, 56, 2024–2043.

[5] Huang G.-H., Wang C.-K., Multi-scale Geostatistical estimation of gravel-bed roughness from terrestrial and airborne laser scanning. IEEE Geosci. Remote Sens. Lett., 2012, 9,1084–1088.

[6] Qin J., Zhong D., Wang G., S.L. Ng, Influence of particle shape on surface roughness: Dissimilar morphological structures formed by man-made and natural gravels. Geomorphology, 2013, 190, 16–26.

[7] Robert A., Statistical properties of sediment bed profiles in alluvial channels. Math. Geol., 1988, 20, 205–225.

[8] Heritage G.L., Milan D.J., Terrestrial laser scanning of grain roughness in a gravel-bed river. Geomorphology, 2009, 113, 4–11.

[9] Hodge R., Brasington J., Richards K., In situ characterization of grain-scale fluvial morphology using Terrestrial Laser Scanning. Earth Surf. Proc. Land., 2009b, 36, 954–968.

[10]Picco L., Mao L., Cavallli M., Buzzi E., Rainato R., Lenzi M.A., Evaluating short-term morphological changes in a gravel-bed braided river using terrestrial laser scanner. Geomorphology, 2013, 201, 323–334.

[11]Wang C.-K., Wu F.-C., Huang G.-H., Lee C.-Y., Meso-scale Terrestrial Laser Scanning of Fluvial Gravel Surfaces. IEEE Geosci. Remote Sens. Lett., 2011, 8, 1075-1079.

[12]Hohenthal, J., P. Alho, J. Hyyppä, and H. Hyyppä, Laser scanning applications in fluvial studies. Prog. Phys. Geogr., 2011, 35, 782–809.

[13]Legleiter C.J., Remote measurement of river morphology via fusion of LiDAR topography and spectrally based bathymetry. Earth Surf. Proc. Land., 2012, 37, 499–518.

[14]Tamminga A.D., Eaton B.C., Hugenholtz C.H., UAS-based remote sensing of fluvial change following an extreme flood event. Earth Surf. Proc. Land., 2015, DOI: 10.1002/esp.3728.

[15]Westaway R., Lane S.N., Hicks D.M., Remote survey of large-scale braided, gravel-bed rivers using digital photogrammetry and image analysis. Int. J. Remote Sens., 2003, 24, 795–815.

[16]Woodget A.S., Carbonneau P.E., Visser F., Maddock I.P., Quantifying submerged fluvial topography using hyperspatial resolution UAS imagery and structure from motion photogrammetry. Earth Surf. Proc. Land., 2015, 40, 47–64.

[17]Atkinson P.M., Resolution manipulation and sub-pixel mapping in Remote Sensing Image Analysis: Including the Spatial Domain, S.M. de Jong and F.D. van der Meer (eds). Kluwer Academic, Dordrecht, 2004, 51–70.

[18]Journel A.G., Huijbregts C.J., Mining geostatistics. 1978, Academic Press, London.

[19]Webster R., Oliver M.A., Geostatistics for Environmental Scientists. 2007, Wiley.

[20]van der Meer F., Remote-sensing image analysis and geostatistics. Int. J. Remote Sens., 2012, 33, 5644–5676.

[21]Wen, R., and R. Sinding-Larsen, Image filtering by factorial kriging-sensitivity analysis and application to gloria side-scan sonar images. Math. Geol., 1997, 29, 433–468.

[22]Wu, F.-C., C.-K. Wang, G.-H. Huang, Delineation of gravel-bed clusters via factorial kriging. Geomorphology, 2018, 308, 161–174.

[23]Oliver, M. A., R. Webster, and K. Slocum, Filtering SPOT imagery by kriging analysis. Int. J. Remote Sens., 2000, 21, 735–752.

[24]Goovaerts P., Sonnet P., Navarre A., Factorial kriging analysis of spring water contents in the dyle river basin, Belgium. Water Resour. Res., 1993, 29, 2115–2125.

[25]Yao T., Mukerji T., Journel A., Mavko G., Scale matching with factorial kriging for improved porosity estimation from seismic data. Math. Geol., 1999, 31, 23–46.

[26]Goovaerts P., Jacquez G.M., Greiling D., Exploring scale-dependent correlations between cancer mortality rates using factorial kriging and population-weighted semivariograms. Geogr. Anal., 2005, 37, 152–182.

[27]Huang G.-H., Wang C.-K., Wu F.-C., Atkinson P.M., Anisotropy characteristics of exposed gravel beds revealed in high-point-density airborne laser scanning data. IEEE Geosci. Remote Sens. Lett., 2016, 13,1044–1048.

[28]Shan J., Toth C.K., Topographic Laser Ranging and Scanning: Principles and Processing. 2008, CRC Press.

[29]Jutzia B., Stillab U., Range determination with waveform recording laser systems using a Wiener Filter. ISPRS J. Photogramm. Remote Sens., 2006, 61, 95–107.

448 [30]Cavalli M., Tarolli P., Marchi L., Fontana G.D., The effectiveness of airborne LiDAR data in
449 the recognition of channel-bed morphology. Catena, 2008, 73, 249– 260.

450 [31]Glenn N. F., Streutker D.R.,. Chadwick D.J, Thackray G.D., Dorsch S.J., Analysis of LiDAR-
451 derived topographic information for characterizing and differentiating landslide morphology
452 and activity. Geomorphology, 2006, 73, 131–148.

453 [32]Patrick L.W., Glaze L.S., Calder E.S., Harding D.J., LiDAR-derived surface roughness texture
454 mapping: application to Mount St. Helens Pumice Plain deposit analysis. IEEE Trans. Geosci.
455 Remote Sens., 2014, 52, 426–438.

456 [33]Rameshwaran P., Naden P.S., Lawless M., Flow modelling in gravel-bed rivers: rethinking the
457 bottom boundary condition. Earth Surf. Proc. Land., 2011, 36, 1350–1366.

458 [34]Bathrellos G.D., Vasilatos C., Skilodimou H.D., Stamatakis M.G., On the occurrence of a
459 pumice-rich layer in Holocene deposits of western Peloponnesus, Ionian Sea, Greece. A
460 geomorphological and geochemical approach. Open Geosciences, 2009, 1(1), 19–32.

Figure

Illustrations

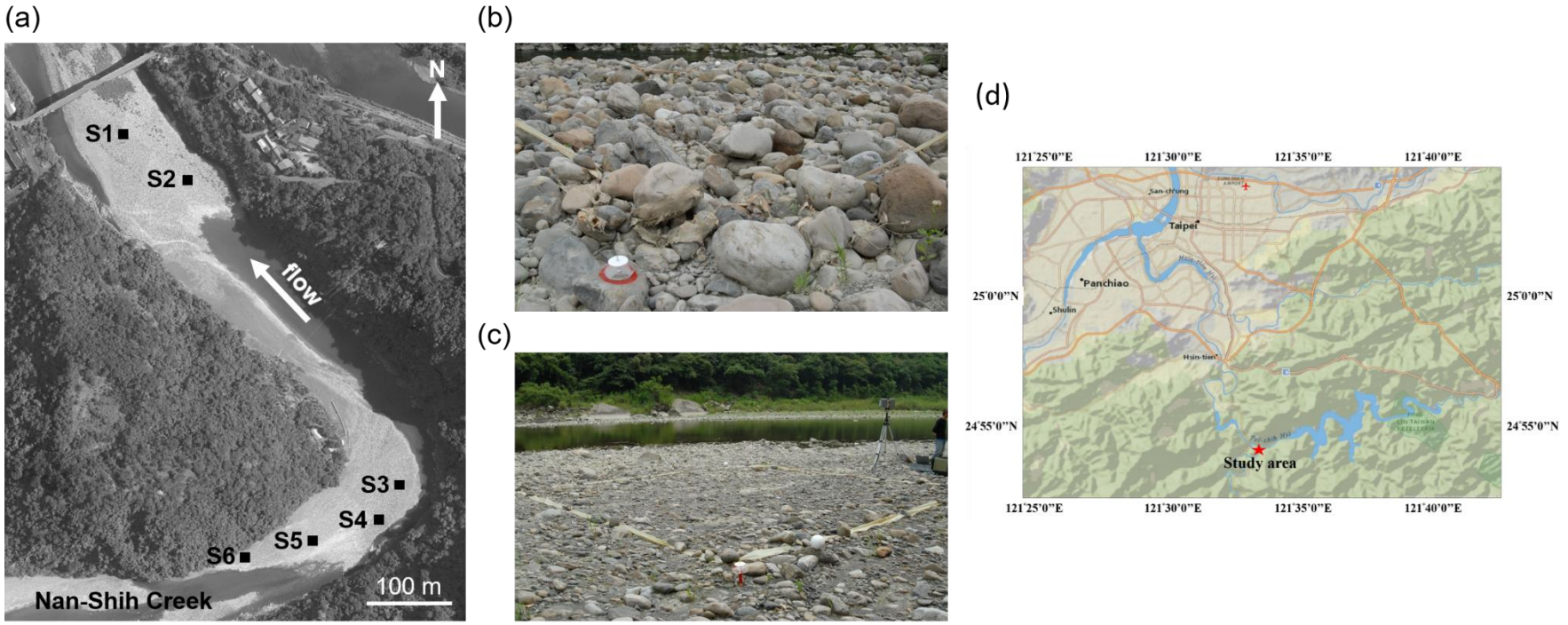

Figure 1. (a) Georectified orthophoto with a spatial resolution of 5 cm × 5 cm showing the study area near the confluence of Nan-Shih Creek and Pei-Shih Creek, northern Taiwan, with a latitude and longitude of 24°54'10"N and 121°33'24"E, respectively. The six gravel bed sites for TLS survey are denoted S1 to S6. (b) and (c) are the field photos of S4 and S6, respectively. (d) Location map of study area.

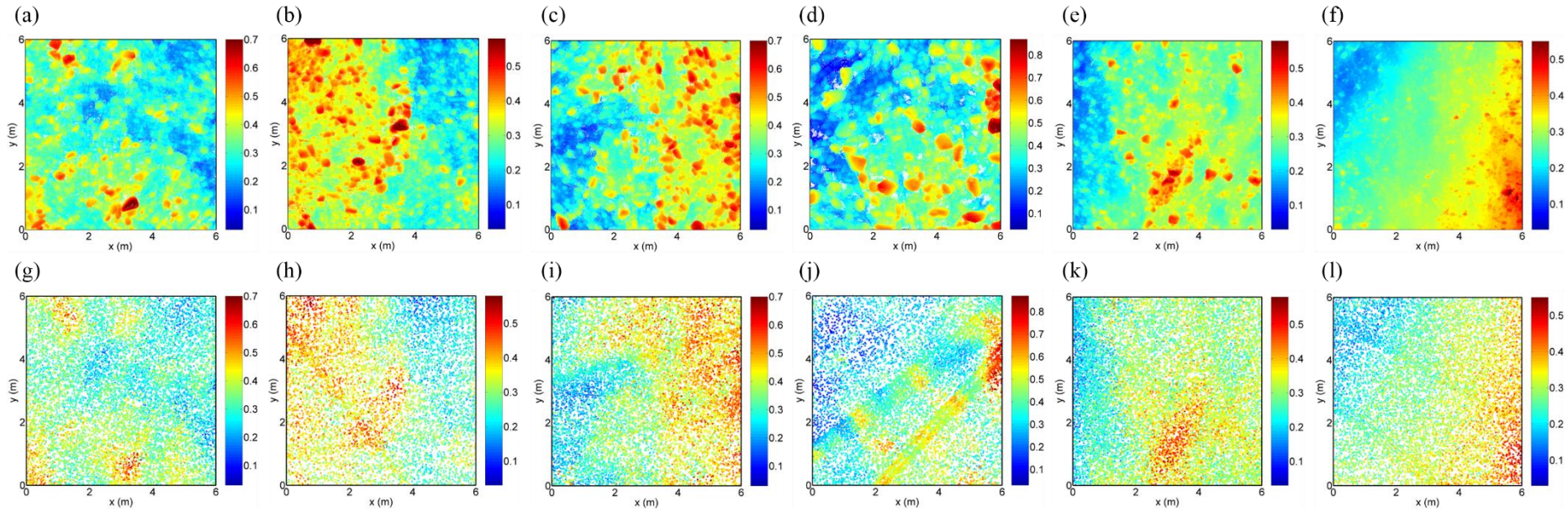

Figure 2. Colour maps showing TLS-derived DSMs: (a) S1, (b) S2, (c) S3, (d) S4, (e) S5, and (f) S6 (units: meters). Colour maps showing ALS point clouds: (g) S1, (h) S2, (i) S3, (j) S4, (k) S5, and (l) S6 (units: meters).

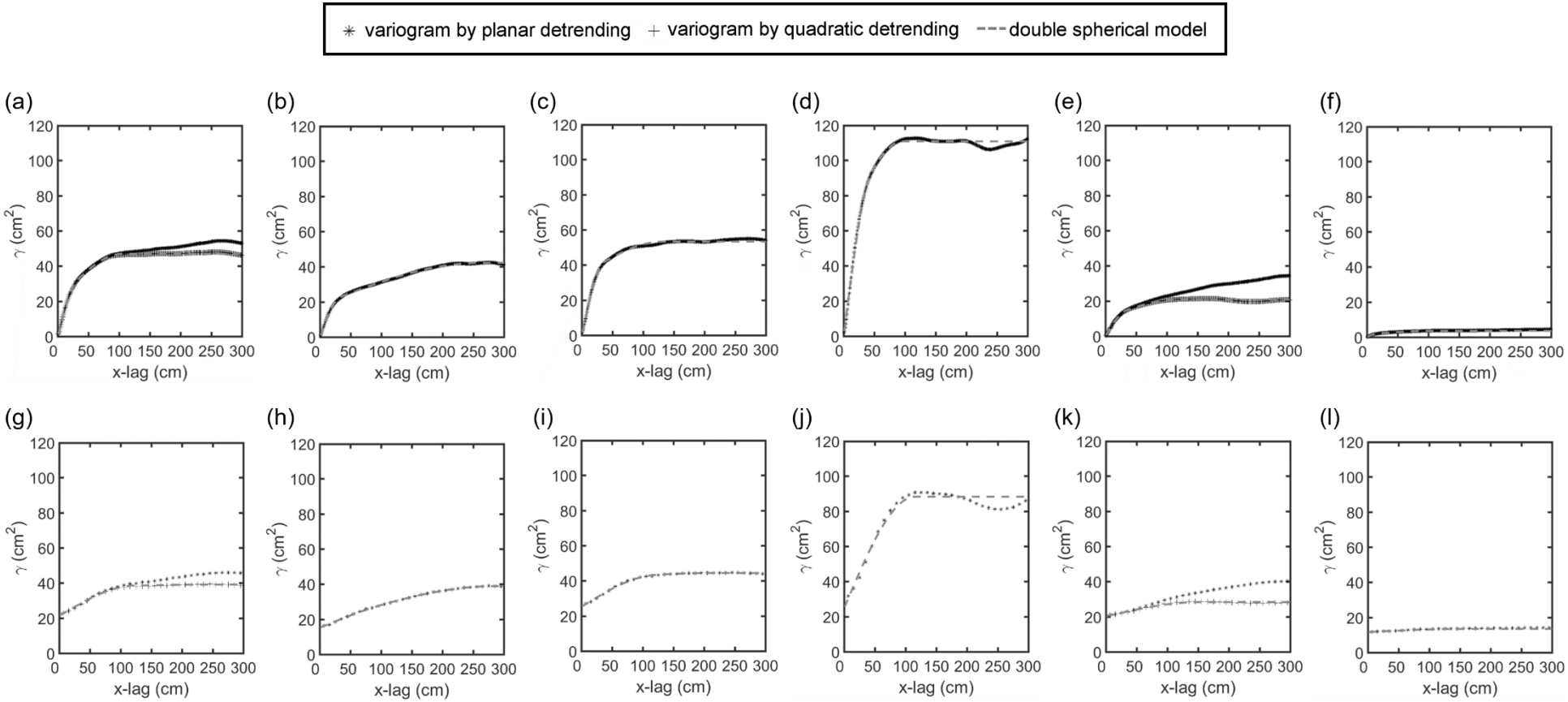

Figure 3. Empirical variograms of TLS-derived DSMs: (a) S1, (b) S2, (c) S3, (d) S4, (e) S5, and (f) S6. Empirical variograms of ALS point clouds: (g) S1, (h) S2, (i) S3, (j) S4, (k) S5, and (l) S6.

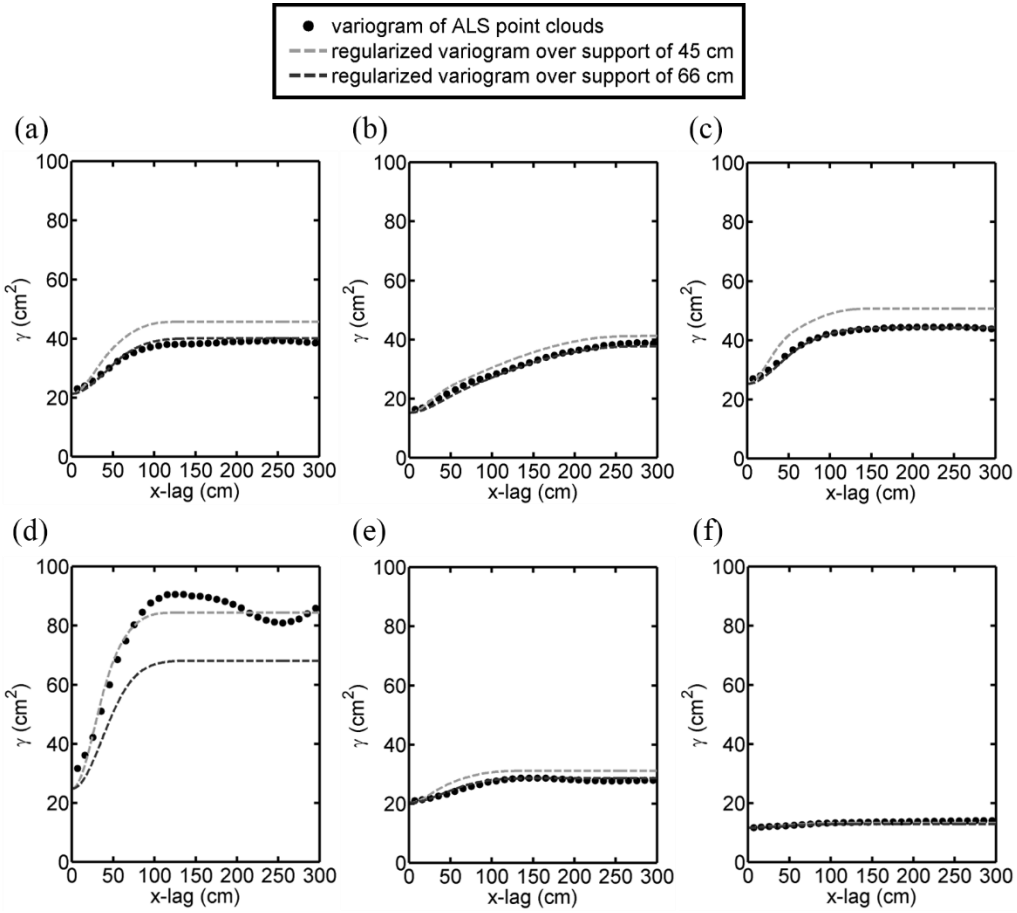

Figure 4. Comparison of the regularized TLS variogram and the observed variogram of ALS point clouds: (a) S1, (b) S2, (c) S3, (d) S4, (e) S5, and (f) S6.

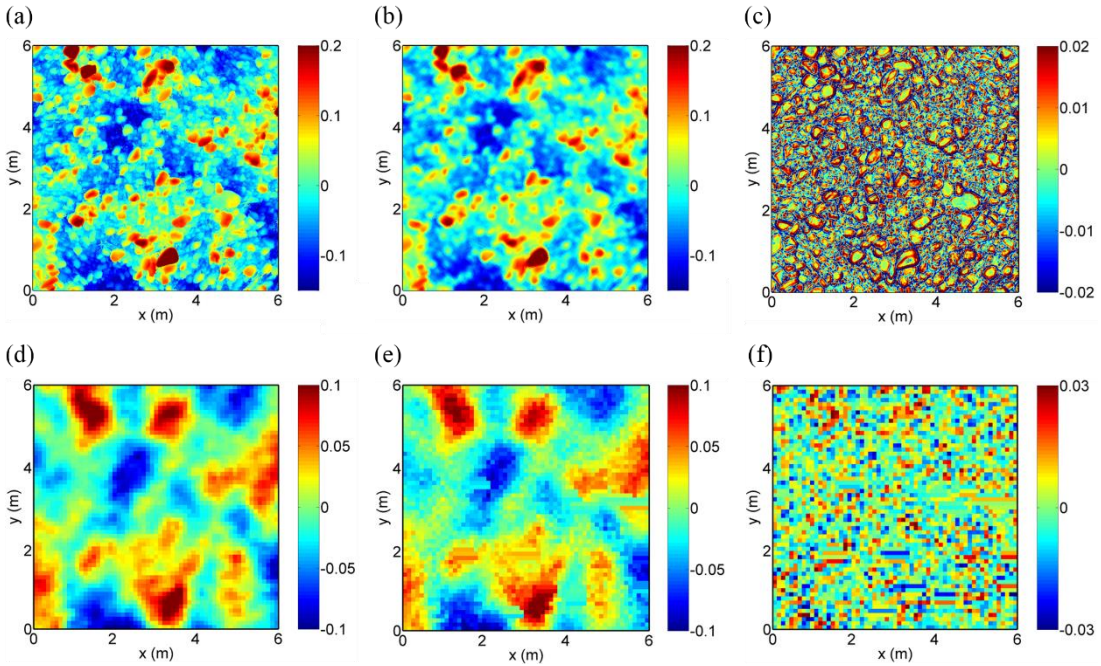

Figure 5. S1: OK map calculated from (a) TLS-derived DSM and (d) ALS point clouds. Long-range FK maps calculated from (b) TLS-derived DSM and (e) ALS point cloud. Short-range FK maps calculated from (c) TLS-derived DSM and (f) ALS point clouds.

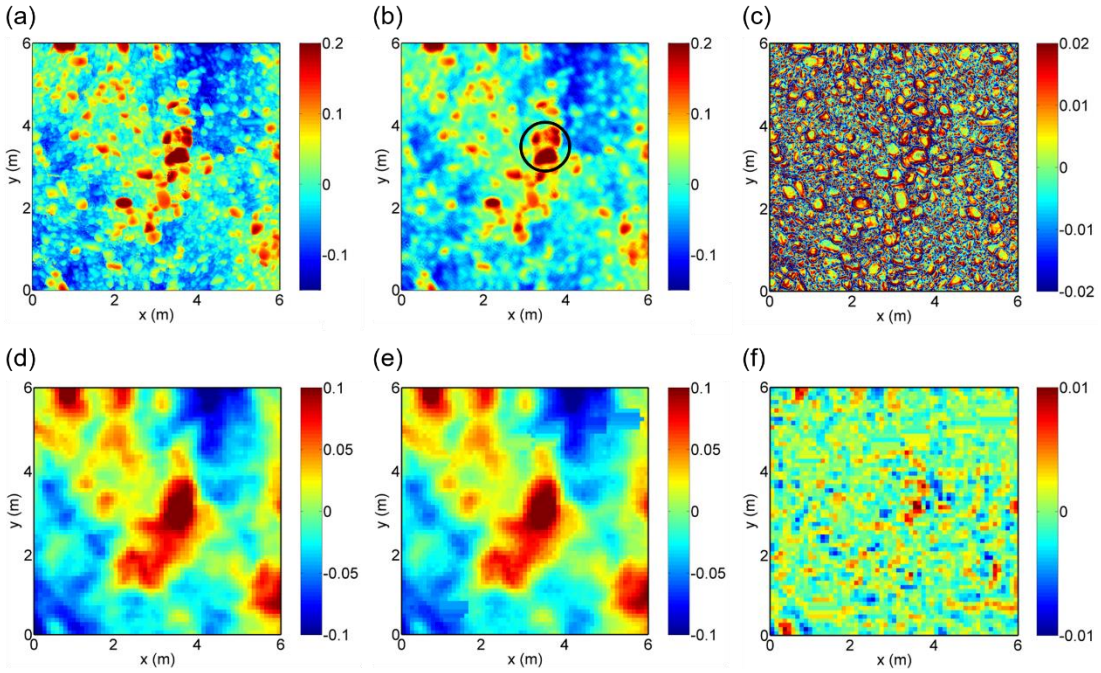

Figure 6. S2: OK map calculated from (a) TLS-derived DSM and (d) ALS point clouds. Long-range FK maps calculated from (b) TLS-derived DSM and (e) ALS point cloud. Short-range FK maps calculated from (c) TLS-derived DSM and (f) ALS point clouds. The black circle in (b) represents ring clusters.

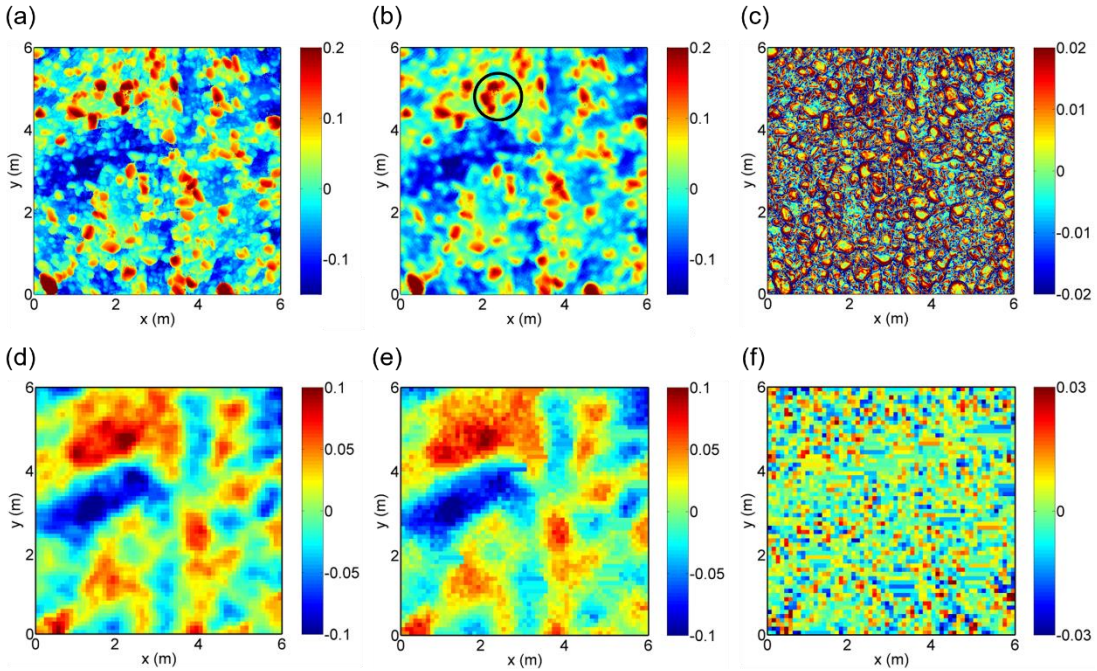

Figure 7. S3: OK map calculated from (a) TLS-derived DSM and (d) ALS point clouds. Long-range FK maps calculated from (b) TLS-derived DSM and (e) ALS point cloud. Short-range FK maps calculated from (c) TLS-derived DSM and (f) ALS point clouds. The black circle in (b) represents ring clusters.

Tables

Table 1: Parameters of the Theoretical Variograms for S1-S6 (Units: meter)

Site	TLS-derived DSM					ALS data				
	C_0	C_1	a_1	C_2	a_2	C_0	C_1	a_1	C_2	a_2
S1	0.00	2.0×10^{-3}	0.32	2.7×10^{-3}	1.05	2.1×10^{-3}	1.6×10^{-3}	1.23	0.1×10^{-3}	2.70
S2	0.00	1.8×10^{-3}	0.33	2.4×10^{-3}	2.59	1.5×10^{-3}	0.2×10^{-3}	1.07	2.2×10^{-3}	2.86
S3	0.00	3.4×10^{-3}	0.37	1.9×10^{-3}	1.32	2.5×10^{-3}	1.5×10^{-3}	1.20	0.5×10^{-3}	2.10
S4	0.00	6.0×10^{-3}	0.46	5.1×10^{-3}	0.96	2.5×10^{-3}	6.3×10^{-3}	1.15	NA	NA
S5	0.00	1.0×10^{-3}	0.34	1.1×10^{-3}	1.15	2.0×10^{-3}	0.8×10^{-3}	1.54	NA	NA
S6	0.00	0.2×10^{-3}	0.18	0.2×10^{-3}	1.11	1.2×10^{-3}	0.2×10^{-3}	1.50	NA	NA

* C_0 is the nugget component, C_1 and C_2 are the partial sills of the first and second model, respectively, a_1 and a_2 are the range parameters of the first and second model, respectively.